

Article

Unsteady-State CO₂ Foam Generation and Propagation: Laboratory and Field Insights

Zachary Paul Alcorn *, Aleksandra Sæle, Metin Karakas and Arne Graue

Department of Physics and Technology, University of Bergen, 5009 Bergen, Norway

* Correspondence: zachary.alcorn@uib.no

Abstract: This work presents a multiscale experimental and numerical investigation of CO₂ foam generation, strength, and propagation during alternating injection of surfactant solution and CO₂ at reservoir conditions. Evaluations were conducted at the core-scale and with a field-scale radial simulation model representing a CO₂ foam field pilot injection well. The objective of the experimental work was to evaluate foam generation, strength, and propagation during unsteady-state surfactant-alternating-gas (SAG) injection. The SAG injection rapidly generated foam based upon the increased apparent viscosity compared to an identical water-alternating-gas (WAG) injection, without surfactant. The apparent foam viscosity of the SAG continually increased with each subsequent cycle, indicating continued foam generation and propagation into the core. The maximum apparent viscosity of the SAG was 146 cP, whereas the maximum apparent viscosity of the WAG was 2.4 cP. The laboratory methodology captured transient CO₂ foam flow which sheds light on field-scale CO₂ foam flow. The single-injection well radial reservoir simulation model investigated foam generation, strength, and propagation during a recently completed field pilot. The objective was to tune the model to match the observed bottom hole pressure data from the foam pilot and evaluate foam propagation distance. A reasonable match was achieved by reducing the reference mobility reduction factor parameter of the foam model. This suggested that the foam generated during the pilot was not as strong as observed in the laboratory, but it has propagated approximately 400 ft from the injection well, more than halfway to the nearest producer, at the end of pilot injection.

Keywords: foam; CO₂; EOR; multiscale

Citation: Alcorn, Z.P.; Sæle, A.; Karakas, M.; Graue, A. Unsteady-State CO₂ Foam Generation and Propagation: Laboratory and Field Insights. *Energies* **2022**, *15*, 6551. <https://doi.org/10.3390/en15186551>

Academic Editors: Daoyong Yang, Shengnan Chen, Huazhou Li, Yin Zhang, Xiaoli Li and Zhaoqi Fan

Received: 18 August 2022

Accepted: 3 September 2022

Published: 7 September 2022

Publisher's Note: MDPI stays neutral with regard to jurisdictional claims in published maps and institutional affiliations.



Copyright: © 2022 by the authors. Licensee MDPI, Basel, Switzerland. This article is an open access article distributed under the terms and conditions of the Creative Commons Attribution (CC BY) license (<https://creativecommons.org/licenses/by/4.0/>).

1. Introduction

Foam has emerged as a promising, cost effective technique to reduce CO₂ mobility for improved sweep efficiency during CO₂ enhanced oil recovery (EOR) and CO₂ storage processes [1–4]. Foam is a dispersion of gas in a continuous liquid phase where gas flow is impeded by thin liquid films called lamellae [5,6]. Lamellae are often stabilized by water-soluble surfactants which reduce surface tension and are screened to ensure minimal adsorption on reservoir rock. Foam is generated in-situ by simultaneous injection of CO₂ and surfactant solution (co-injection) or in alternating slugs of CO₂ and surfactant solution [7,8]. Once foam is generated, it is propagated through the porous medium at an initial unsteady-state and then later at steady-state. Unsteady-state foam is characterized by a rapidly increasing pressure drop, whereas the pressure drop is constant at steady-state and can be described with Darcy's Law [9,10]. In addition, significant differences in relative permeability have been observed between steady- and unsteady-state foam flow [11]. At the field scale, it is assumed that foam is at steady-state [12]. However, foam may encounter both unsteady-state and steady-state flow regimes, with unsteady-state flow dominating the near wellbore area.

Foam injection must balance injectivity, mobility reduction, and operational constraints. At laboratory scale, co-injection is the most common injection strategy because of the ability to achieve steady-state and for deriving foam model parameters [13]. In addition,

co-injection offers the most control of injected foam quality [14]. However, co-injection can be challenging at the field-scale because of operational limitations, extremely low injectivities, rapid pressure increases, and challenges associated with downhole corrosion [15]. This has led to most field tests using a surfactant-alternating-gas (SAG) injection strategy. Additionally, SAG processes have been shown to be the optimal injection strategy to overcome gravity override and to maintain injectivity [16].

Details on in-situ foam generation and propagation during unsteady-state flow are needed because they significantly impact injectivity, which is crucial to the success of foam applications for EOR and CO₂ storage. However, few attempts have been made to characterize transient CO₂ foam behavior during alternating injection of surfactant solution and CO₂ slugs at reservoir conditions. Moreover, the connection between laboratory and field-scale transient foam flow is unclear. To further complicate the matter, conventional reservoir simulations calculate injectivity assuming a uniform saturation and mobility in the injection-well grid block. Therefore, injectivity in a simulation of an SAG process is extremely poor [17]. In reality, foam in the near-well region rapidly dries out and injectivity is much greater than estimated in a finite-difference simulation. Foam dry-out occurs at high gas fractional flows due to foam coalescence and depletion of adequate surfactant solution. The large injectivity reduction can be compounded by limited variation in foam apparent viscosity at different gas fractions from experimental data used to derive foam model parameters. Therefore, an approach to capture foam dry-out in the near-well region is needed.

This work presents a multiscale investigation of unsteady-state CO₂ foam generation, strength, and propagation at reservoir conditions. The main objective of the experimental work was to evaluate foam generation and propagation during unsteady-state SAG injection at reservoir conditions to assist with field pilot interpretations. The aim was to develop a laboratory methodology for CO₂ foam quantification during SAG injection, representative of the near wellbore region. The objective of the field-scale modeling work was to calibrate a radial reservoir simulation model to the observed behavior from a recently completed CO₂ foam field pilot test. An approach to capture the foam dry-out effect near the well is proposed.

2. Pilot Overview

A surfactant-stabilized CO₂ foam pilot was conducted in a mature heterogeneous carbonate reservoir in East Seminole Field, Permian Basin USA [18]. The main objective was to achieve in-depth CO₂ mobility control to increase CO₂ sweep efficiency and improve the CO₂ utilization factor. The foam formulation was designed in the laboratory by measuring surfactant adsorption and verifying foam stability in the presence of residual oil [19–21].

The pilot area was an inverted 40 acre five-spot pattern with a central injection well and four surrounding producers. The pilot injection strategy was designed to mitigate injectivity losses due to strong foam generation and to volumetrically target the optimal 70% foam quality, as recommended from the laboratory studies. A rapid surfactant-alternating-gas (SAG) injection strategy began in May 2019. The injection strategy consisted of SAG cycles with 10 days of surfactant solution injection followed by 20 days of CO₂ injection. Eleven complete SAG cycles were injected for total of 10% hydrocarbon pore volume (HCPV) injected at the completion of the pilot in August 2020. Figure 1 shows the observed injection rates and bottom hole pressure (BHP) during the pilot.

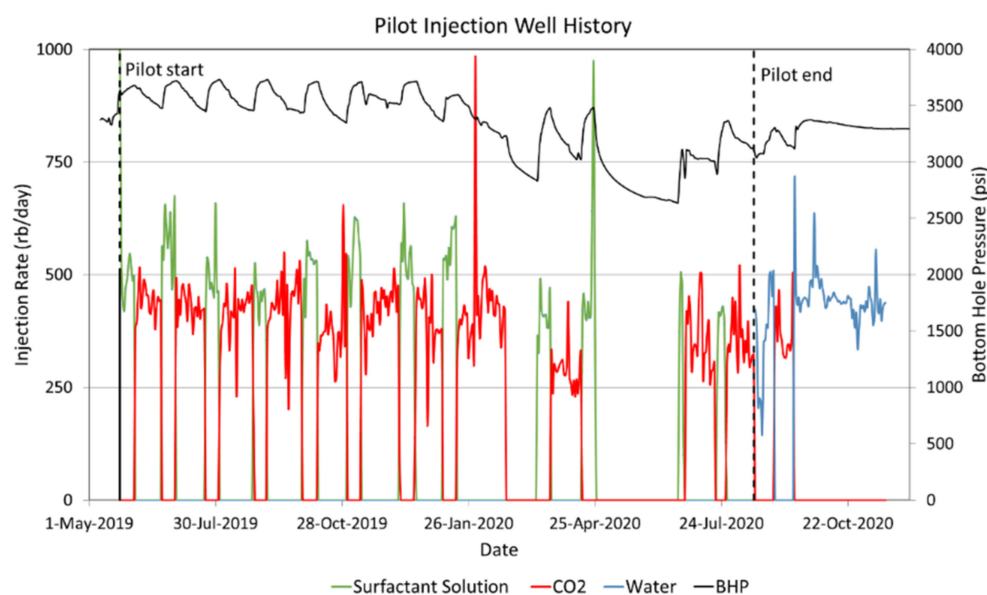


Figure 1. Observed injection rates and bottom hole pressure (BHP) during the foam pilot. The red curve corresponds to CO₂ injection, the green curve to surfactant solution injection, and the blue to water injection. The BHP is shown as the black curve.

Pilot Monitoring

The baseline data collection and pilot monitoring program aimed to obtain baseline from pre-pilot CO₂ and water injection periods and monitor pilot performance to evaluate reservoir response to foam injection. Foam was expected to reduce CO₂ mobility, thus the baseline period focused on characterizing interwell connectivity and injectivity of CO₂ and water. The baseline data collection program consisted of CO₂ injection profile logs, an interwell CO₂ tracer test (IWTT) and collection of injection and production flow rates for comparison to repeat surveys during the pilot. The pilot monitoring program included repeat CO₂ injection profiles, an IWTT, three-phase production monitoring and collection of downhole pressure data for evaluation of reservoir response to foam injection. The injection bottom hole pressure and temperature were monitored by mounting a downhole pressure gauge (DHPG) in the pilot injection well. Produced fluids were also collected, before the pilot and once a week during the pilot, for chemical analysis to determine surfactant breakthrough time.

Foam generation was confirmed during the pilot based upon a delay in CO₂ breakthrough compared to the baseline CO₂ breakthrough time, higher BHP values during the pilot compared to pre-pilot values, and more evenly distributed injection profiles during the pilot compared to the pre-pilot period. In addition, an increase in oil production was observed with less volumes of CO₂ injected during the pilot, compared to conventional CO₂ injection, thereby improving the CO₂ utilization factor and the economics of the project. Pilot results are discussed in detail in [22]. Observed BHP values and injection rates were used in this work to calibrate the radial reservoir model as discussed below.

3. Experimental Materials

The objective of the unsteady-state CO₂ foam experiments was to evaluate foam generation, strength, and collapse during alternating injection of CO₂ and surfactant solution to assist in the interpretation of the recently completed field pilot. The aim was to develop a laboratory methodology for CO₂ foam quantification during unsteady-state SAG injection, representative of the near wellbore region.

3.1. Rock and Fluid Properties

An outcrop Bentheimer sandstone was used for all experiments to maintain constant core properties. Bentheimer is a homogeneous, water-wet sandstone with a composition consisting of quartz (92%), clay minerals (3%) and feldspar (5%). The permeability was measured at an average of 2.14 ± 0.03 Darcy. Rock properties are shown in Table 1.

Table 1. Rock properties of the sandstone core material used in the experimental work.

Property	Value
Length (cm)	24.40 ± 0.01
Diameter (cm)	3.80 ± 0.01
Permeability (D)	2.14 ± 0.03
Pore Volume (mL)	62.16 ± 0.01
Porosity (%)	21.54 ± 0.10

Brine was prepared by dissolving 3.5 wt.% NaCl and distilled water. The foaming agent was a nonionic surfactant from Huntsman, SURFONIC L24-L22, that was dissolved in brine. The surfactant concentration was 0.50 wt% as also used in the pilot test. The SURFONIC L24-L22 surfactant demonstrated low adsorption in carbonate rock material, both in the absence and presence of CO₂ [19]. In addition, it is expected to have low adsorption on the surface of the Bentheimer sandstone. CO₂ of 99.999% purity was used during the foam injections. Isopropyl alcohol solution consisting of 87.5 wt.% isopropyl and 3.5 wt.% distilled water was injected to clean the core between each experiment. See Table 2 for an overview of fluid compositions used in the experimental work.

Table 2. Properties of the fluids used in the experimental work.

Fluid	Composition
Brine	Distilled water + 3.5 wt% NaCl
Surfactant solution	Brine + 0.5 wt% SURFONIC L24-L22
CO ₂	>99.999% CO ₂
Isopropyl alcohol	Distilled water + 87.5 wt% Di-propanol

3.2. Experimental Setup

Figure 2 shows a schematic of the experimental setup used for the unsteady-state CO₂ foam experiments. The temperature and pressure were set to reservoir conditions of 40 °C and 198 bar. The core was wrapped in a layer of nickel foil and placed inside of a Teflon rubber sleeve to prevent CO₂ diffusion into the sleeve [23]. The core was then inserted into a vertically-oriented Hassler core holder. The system was pressurized by an N₂ tank connected with two Equilibar back pressure regulators (BPR) connected in series to reduce fluctuations and keep a constant pressure in the system. An ISCO pump kept the confinement pressure 70 bar over the system pressure. The confinement pressure, pressure at the inlet and outlet of the core and the pressure over the BPRs were measured and monitored by ESI-pressure transducers (Figure 2). The differential pressure over the core was used to calculate foam apparent viscosity and was measured by Aplisens Smart Differential Pressure Transmitter.

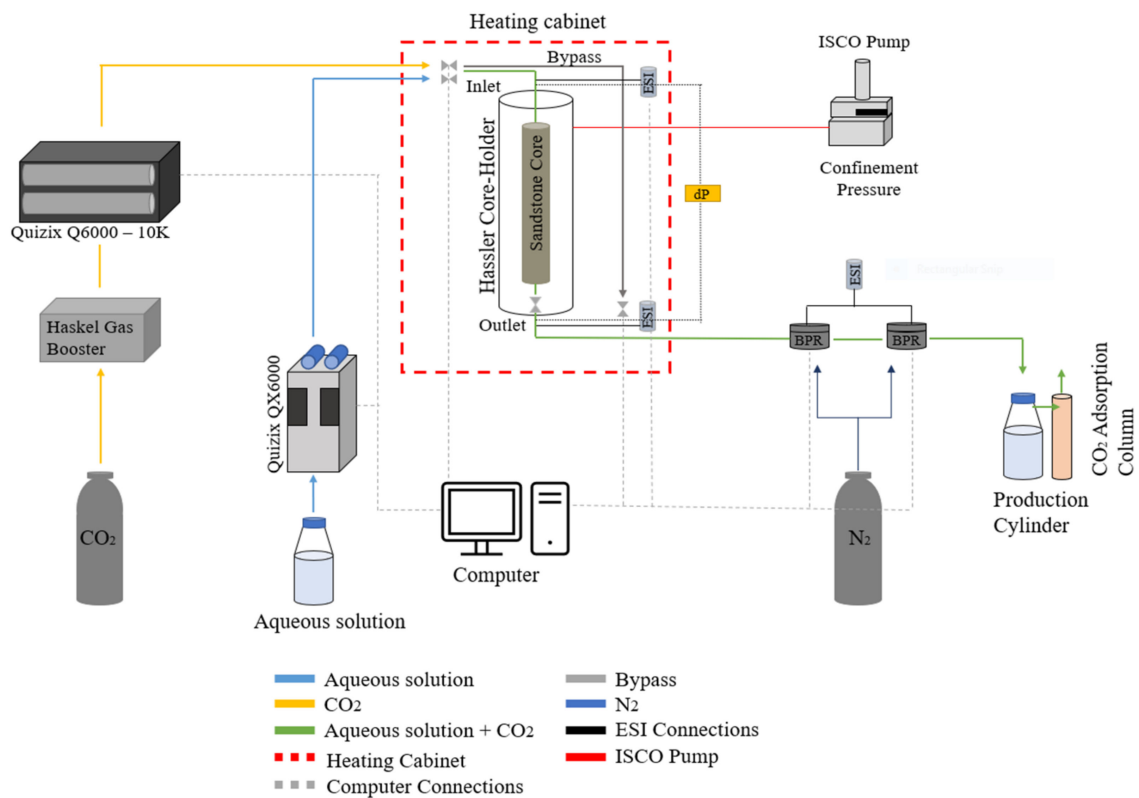


Figure 2. Illustration of experimental setup used for unsteady-state foam injections.

The aqueous solutions were injected through a Quizix QX6000-pump and CO₂ was injected through a Quizix Q6000-10K pump. CO₂ was pressurized by a Haskel gas booster to achieve a supercritical phase before it was injected through the pump and into the core. The production cylinder accumulated the production fluids from the outlet. The fluids were depressurized to atmospheric conditions and CO₂ was separated from the liquid solution by an adsorption column.

4. Experimental Methods

Foam generation, strength and stability were investigated during unsteady-state alternating slug injection of surfactant solution and CO₂. An identical WAG injection (without surfactant) was also conducted to establish a baseline for comparison. Foam generation and strength was quantified by calculating apparent viscosity (μ_{app}), which is based on the pressure measured across the core and is defined as:

$$\mu_{app} = \frac{k}{\mu_{gas} + \mu_{liquid}} \nabla p, \quad (1)$$

where k is the absolute permeability of the core, μ_{gas} and μ_{liquid} are the superficial velocities of gas and liquid, respectively, and ∇p is the pressure gradient across the core [24]. A higher apparent viscosity value corresponds to a stronger foam and increased resistance to flow.

The experimental procedure and injection strategy were designed to represent unsteady-state flow in the near wellbore region. The experimental procedure for the baseline water-alternating-gas (WAG) and surfactant-alternating-gas (SAG) are shown in Figure 3 and are discussed below.

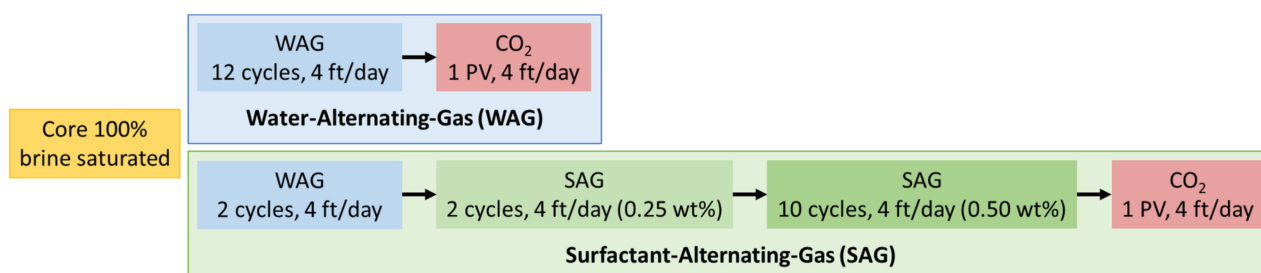


Figure 3. Experimental injection sequence for the baseline water-alternating-gas (WAG) and the surfactant-alternating-gas (SAG). The core was initially 100% saturated with brine and all injection rates were 4 ft/day. Individual WAG or SAG cycles injected 0.25 pore volumes (PV).

4.1. Baseline Water Alternating Gas (WAG)

The core was initially 100% saturated with brine by injecting brine at a low rate for five pore volumes (PV). The WAG injection was then conducted by injecting alternating slugs of brine and CO₂ at an injection rate of 4 ft/day. One brine slug and one CO₂ slug comprised one complete WAG cycle. The WAG injection procedure first injected brine for 0.10 PV. Next, the first CO₂ slug was injected for 0.15 PV to achieve the targeted 0.60 gas fraction. The WAG injection procedure was repeated until 12 complete WAG cycles were injected. Continuous CO₂ was then injected for 1 PV to study foam dry-out.

4.2. Surfactant Alternating Gas (SAG)

The core was initially 100% saturated with brine by injecting brine at a low rate for 5 PV. An initial 2-cycle WAG was conducted, followed by a diluted 2-cycle SAG and finally a 10-cycle SAG with 0.50 wt% surfactant solution. Pure CO₂ was injected at the end of the experiment for 1 PV. All injection rates were 4 ft/day at a gas fraction of 0.60, identical to the baseline WAG injection.

5. Modeling Methods

A single injection well radial reservoir simulation model was set up to investigate foam generation, strength, and propagation during the field pilot. The objective was to tune the foam model to match the simulated BHP to the observed BHP from the foam pilot. In addition, the sensitivity of foam model parameters on foam generation and propagation were studied. Previous simulation studies with the radial model have also been reported elsewhere [25]. The radial model was based upon a sector scale model that was history matched to the historical water and CO₂ injection periods in East Seminole Field [26].

The radial grid was composed of 560 active grid cells with 28 layers in the z-direction (Figure 4). Cell thicknesses, permeabilities, porosities and saturations were derived from the last step of the history matched sector model. The radial grid was centered around the pilot injection well and grid cell sizes increased logarithmically from the injector to a total of 700 ft. The radial model parameters are shown in Table 3. A commercially available conventional finite-difference compositional reservoir simulator was used for all simulations (ECLIPSE 300). The compositional model utilized the Peng–Robinson (PR) equation of state (EoS) model with six components that were tuned to PVT data. The model included two C7+ components where the lighter components were lumped as CO₂, N₂ + C1, H₂S + C2 + C3, C4 + C5 + C6. Two aqueous phases were included in the model, one for water and one for surfactant. See [26] for a complete description of the fluid model.

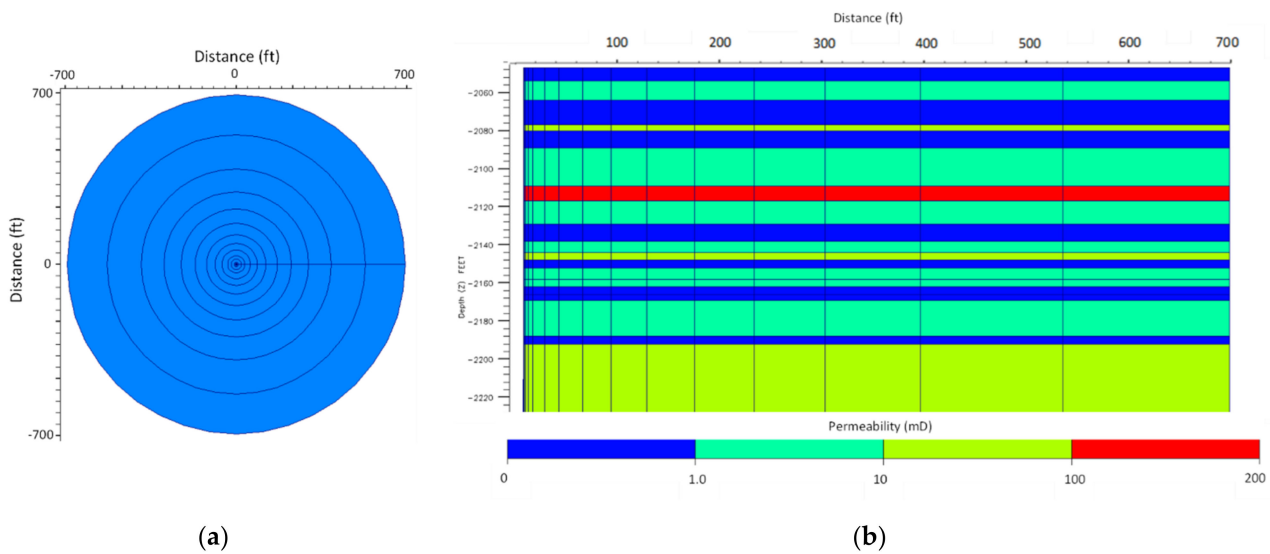


Figure 4. (a) Top view of the radial model. The injection well was placed in the center of the grid. (b) Permeability distribution of a 2D slice (r – z) of the radial simulation model. Properties were derived from the last step of the history matched sector model.

Table 3. Radial model properties.

Parameter	Value
Grid Dimensions (r, θ, z)	$20 \times 1 \times 28$
Outer Radius	700 ft
Total Thickness	145 ft
Initial Water saturation	0.50
Initial Reservoir Pressure	3118 psig
Reservoir Temperature	104 °F
Average Permeability	13.5 mD
Average Porosity	0.08

5.1. Foam Modeling

Foam was modeled with an implicit texture local-equilibrium (LE) model. LE foam models represent the effect of bubble size implicitly by introducing factors for reducing gas mobility by foam as a function of water saturation, oil saturation, surfactant concentration and shear-thinning due to flow rate [27,28]. LE models assume foam is present anywhere gas and water are present along with adequate surfactant concentration.

The decrease in gas mobility during foam floods is accounted for in LE models by scaling the gas relative permeability in the absence of foam (k_{rg}^{nf}) by a mobility reduction factor (FM), whereas the water relative permeabilities remain unchanged.

$$k_{rg}^f = k_{rg}^{nf} \times FM. \quad (2)$$

The effect of water saturation, shear rate, surfactant concentration and oil saturation on mobility reduction factor was modeled, given by the expression:

$$FM = \frac{1}{1 + f_{mmb} \times F_{water} \times F_{shear} \times F_{oil} \times F_{surf}}, \quad (3)$$

where f_{mmb} refers to the maximum gas mobility reduction that can be achieved. Below are the equations for F_{water} , F_{shear} , F_{oil} and F_{surf} which capture the water saturation, shear rate, oil saturation and surfactant concentration dependence, all lying in the range of 0 to 1.

The reduction of gas mobility due to the presence of water is defined as:

$$F_{water} = 0.5 + \frac{\alpha \tan[epdry(S_w - fmdry)]}{\pi}. \quad (4)$$

The capillary number, N_c , describes the relative effect of capillary and viscous forces.

$$F_{shear} = \begin{cases} \left(\frac{fmcap}{N_c}\right)^{epcap} & \text{if } N_c > fmcap \\ 1 & \text{otherwise} \end{cases}. \quad (5)$$

The individual reduction by surfactant concentration indicates that low surfactant concentrations and weak foam results in a low F_{surf} , while higher surfactant concentrations result in a higher individual mobility reduction.

$$F_{surf} = \left(\frac{C_s}{C_s^r}\right)^{epsurf}, \quad (6)$$

where C_s is defined as the surfactant concentration, C_s^r is the surfactant concentration reference and $epsurf$ indicated the rate change when $C_s = C_s^r$.

$$F_{oil} = \left(1 - \frac{S_o}{fmoil}\right)^{epoil}. \quad (7)$$

Foam model parameters ($fmmob$, $fmdry$ and $epdry$) were obtained by fitting the empirical foam model to foam quality scan data through curve fitting regression [13,29]. The base values for $fmcap$ and $epcap$ were obtained by fitting the empirical foam model to rate scan data, assuming $fmmob$, $fmdry$ and $epdry$ to be invariable for regression. Figure 5 shows the model fit to a foam quality and rate scan conducted on a reservoir core at 2500 psi and 104F. The complete experimental procedure for foam quality and rate scans is given in [30].

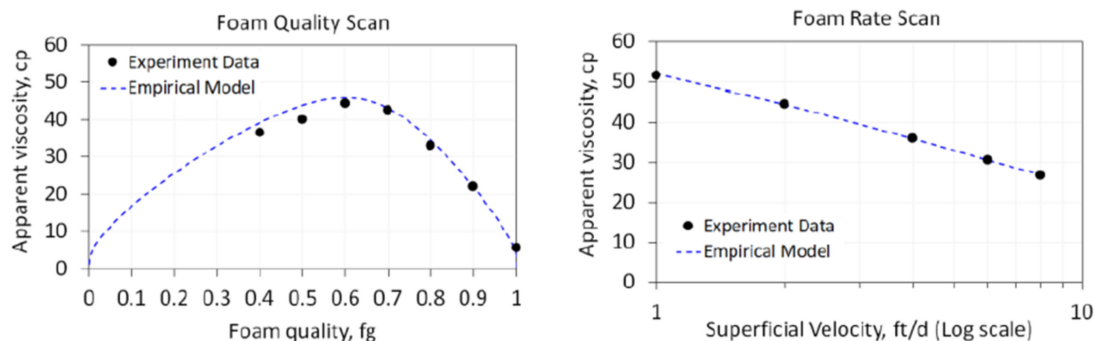


Figure 5. Foam quality scan (left) and foam rate scan (right) for the base case foam model. The empirical foam model (dashed lines) was fit to experimental data (black dots). Modified from [30].

The surfactant selected for the pilot had very low adsorption on the reservoir rock. Therefore, surfactant adsorption was not included in the model. The critical micellar concentration (CMC) was 0.01 wt% (0.035 lb/bbl) for the selected surfactant. The minimum concentration for foam generation was set at CMC, and the reference concentration for transition from weak to strong foam was assumed five times the CMC. The base value of $fmsurf$ was therefore set as 0.05 wt% (0.175 lb/bbl). Due to unavailability of data to characterize the steepness in the change of mobility reduction due to surfactant concentration, the base value of $epsurf$ was assumed 1. Based upon earlier CO₂ foam EOR experiments, the maximum oil saturation above which foam ceased to exit ($fmoil$) was 0.28 [18]. Due to unavailability of data to characterize the steepness in the change of mobility reduction due to oil saturation, the base value of $epoil$ was assumed 1. To model foam dry-out during an SAG process near the injection well, the grid cells connected to the injector were assigned an $fmmob$ of 0. This allowed modeling of a no foam region within a radius of 20 ft around injector to mimic foam dry out near the well.

5.2. Model Initialization

The model was initialized from the last step of the history matched sector model. The simulated injection schedule was identical to the observed injection from the pilot. Figure 6 shows an illustration of the injection schedule. Blue bars correspond to water injection, red to CO₂, and green to surfactant solution injection. The black bars indicate periods of observed field shutdowns that were also included in the simulation schedule. The pre-pilot period (1 April 2019–23 May 2019) included both the historical water injection and CO₂ injection periods. The pilot period (24 May 2019–23 August 2020) was the rapid SAG injection. The post-pilot injection period consisted of a one cycle WAG and then continuous water injection. The model did not capture the effect of nearby production wells on injection BHP because the model contained only the injection well.



Figure 6. Injection overview of the radial model for East Seminole Field. Water injections (blue), CO₂ injections (red), surfactant injections (green), no injection periods (black).

5.3. Baseline Water Alternating Gas (WAG and Base Case Surfactant Alternating Gas (SAG)

A water-alternating-gas (WAG) case was set up to establish a baseline and to determine the CO₂ relative permeability reduction in a WAG process. The baseline WAG case injected only brine (no surfactant) and CO₂ at the targeted gas fraction of 0.70. The injection strategy consisted of 11 complete WAG cycles with alternating slugs of CO₂ for 20 days and water for 10 days. The simulation was run in history match mode where injection rates were set to the observed values from the pilot. The simulated BHP response was compared to the base rapid SAG and to the observed pilot values. The base case SAG was identical to the baseline WAG but included a surfactant component to model foam transport. Base foam model parameters were derived from foam quality and rate scans conducted on reservoir core at reservoir temperature and pressure [30].

5.4. Foam Model Sensitivity Study

The objective of the foam model sensitivity was to investigate the impact of different experimentally derived foam models on foam generation and CO₂ mobility reduction. Injection BHP results were compared to the observed BHP data to determine which foam model best represented foam behavior at the field-scale. All foam model parameters were derived from laboratory foam quality and rate scans as described previously. Three cases were set up with different foam models for the sensitivity study. The foam model parameters are shown in Table 4.

Table 4. Foam model parameters used in the sensitivity study. Foam model 2 was used in the base case.

Model Parameter	1	2 (Base)	3
<i>fmmob</i>	41.5	192	248
<i>fndry</i>	0.595	0.40	0.313
<i>epdry</i>	35	84	46.8
<i>fncap</i>	2.14×10^{-6}	9.00×10^{-7}	8.50×10^{-7}
<i>epcap</i>	0.87	0.59	0.71

The base foam model was used in a sensitivity study of the foam model parameter, *fmmob*. As discussed previously, *fmmob* is the maximum gas mobility reduction that can be achieved with foam. Previous modeling results have shown that this parameter has the most impact on the simulated BHP [25].

6. Results and Discussion

6.1. Experimental: Unsteady-State CO₂ Foam Corefloods

Figure 7 shows apparent viscosity versus pore volume (PV) injected for the first seven cycles (2 PVs injected) of the baseline WAG (blue curve) and the base SAG (green curve). As mentioned previously, the first two cycles for both experiments were WAG cycles which generated no foam. The fluctuation in apparent viscosity between 0 cP and 2 cP during the first two cycles of each experiment was related to reduced CO₂ relative permeability in the presence of high water saturations in a WAG process [31]. The apparent viscosity of the baseline WAG stabilized at an average of 1.66 cP with a maximum value of 2.4 ± 0.2 cP. Therefore, an apparent viscosity of 2.4 cP was used as the foam generation limit for comparison to the SAG experiment (i.e., an apparent viscosity value higher than 2.4 cP indicated foam generation). Once surfactant was injected during the third cycle of the SAG experiment, the apparent viscosity increased above the WAG baseline, indicating foam generation. The apparent viscosity of the SAG continued to increase with each subsequent cycle indicating continued foam generation and propagation into the core.

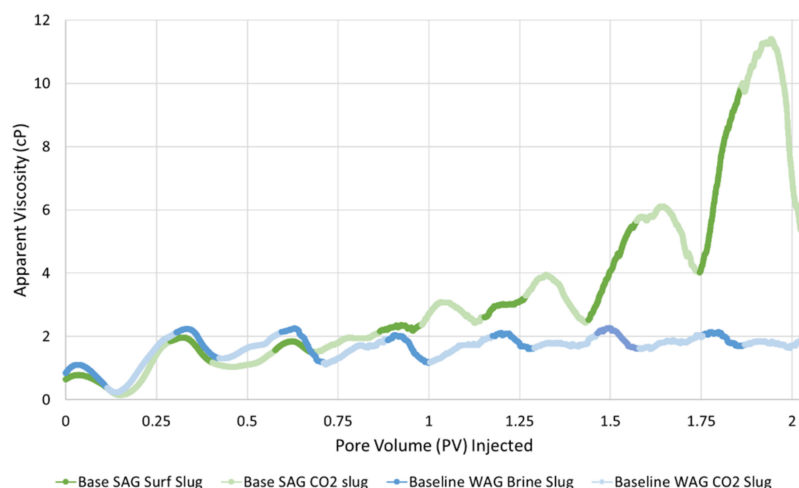


Figure 7. The first seven cycles for the Baseline WAG (blue curve) and Base SAG (green curve) experiments. Surfactant, or water, slugs are indicated with darker colors whereas the CO₂ slugs are lighter colored. The maximum apparent viscosity value of WAG is indicated with the dotted red line.

Figure 8 shows apparent viscosity versus pore volume (PV) injected for the baseline WAG (blue curve) and the base SAG (green curve) for the entire experiment. The apparent viscosity of the base SAG increased continuously from SAG cycle 4 until cycle 12, reaching a peak value of 146 ± 0.4 cP, whereas the baseline WAG had a peak apparent viscosity value of 2.4 ± 0.1 cP.

Foam is usually generated in a drainage-like process where higher capillary pressure results in a snap-off mechanism [32,33]. However, apparent viscosity also increased during surfactant injection (imbibition-like injection). This may be related to foam generation or the viscosity contrast between CO₂ and surfactant solution. The increasing apparent viscosity from cycles 3 until 12 indicated continued foam generation and propagation through the core. The final CO₂ slug was injected for 1 PV to investigate foam stability and foam dry out during a prolonged period of pure CO₂ injection. The highest apparent viscosity value was reached in this slug (146 cP) before foam collapsed due to an effective drainage process, resulting in foam dry-out.

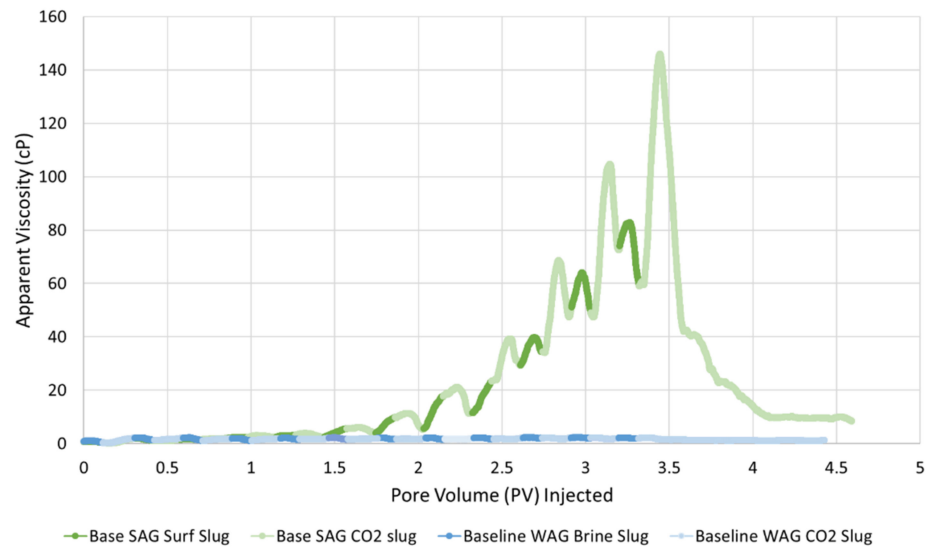


Figure 8. Apparent viscosity versus pore volume (PV) injected for 12 complete cycles for the Baseline WAG (blue curve) and the Base SAG (green curve). Surfactant solution, or water, slugs are indicated with darker colors whereas the CO₂ slugs are lighter colored.

6.2. Radial Model: Baseline WAG and Base Case SAG

The injection BHP of the baseline WAG and base case SAG simulation cases were used to evaluate foam generation and strength with surfactant present. The results were also compared to the observed BHP response from the foam pilot to determine the degree of CO₂ mobility reduction during the pilot. Figure 9 shows the simulated injection BHP through time for the baseline WAG (blue curve) and the base case SAG (green curve). The observed BHP is shown as the black circles. As discussed earlier, the injection well was run in history match mode at a set injection rate that was consistent with the observed injection rate.

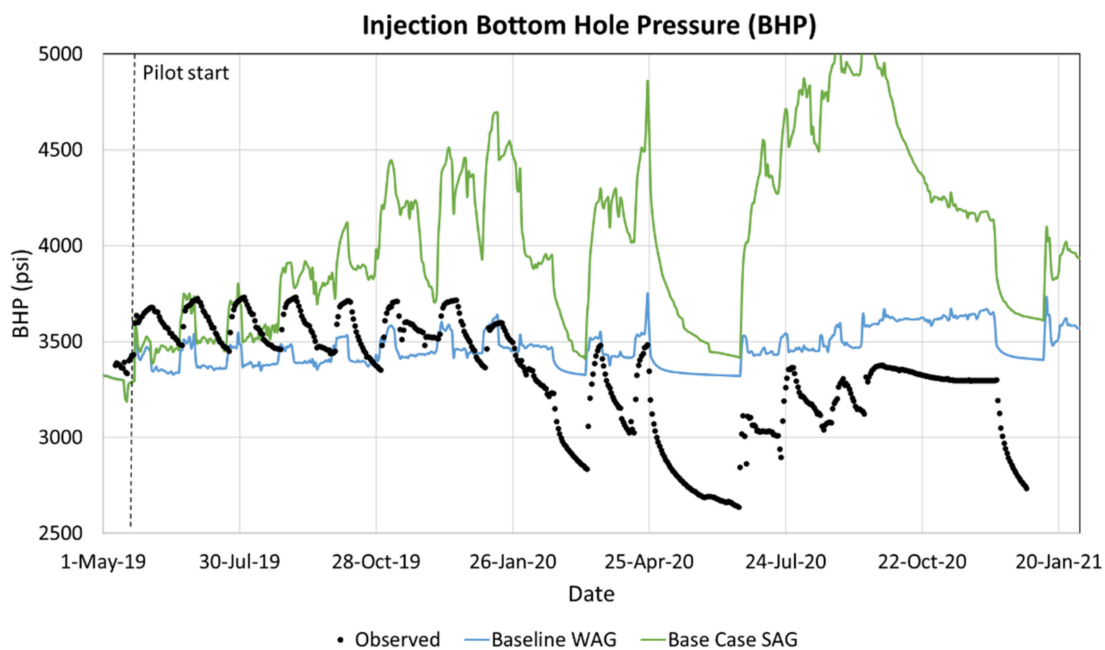


Figure 9. Injection bottom hole pressure (BHP) through time for the baseline WAG (blue curve) and the base case SAG (green curve). The observed BHP is shown as the black circles.

The simulated BHP values for the base case SAG (Figure 9, green curve) were higher than the baseline WAG (Figure 9, blue curve), indicating that foam was generated with surfactant present. Foam generation was also confirmed during the pilot based upon the higher observed BHP values compared to the baseline WAG [21]. However, the base case SAG's BHP values were significantly higher than the observed BHP, especially after the fourth SAG cycle. This suggests that the foam generated during the pilot was not as strong as in laboratory studies as also observed in [25]. In addition, the simulated BHP did not match the observed pressure fall-off after the seventh cycle because the model did not capture the effect of nearby production wells on injection BHP. As mentioned previously, the model contained only the injection well and did not include production that was observed in the field. The increase in BHP during surfactant solution slugs and subsequent decrease during CO₂ slug injection may be related to the viscosity difference between CO₂ and surfactant solution at these conditions. However, it may also be related to increased CO₂ injectivity due to water displacement in the near well area during CO₂ injection [34]. Indeed, the decreased BHP during CO₂ slugs, compared to surfactant solution slugs, at the same injection rates, increased CO₂ injectivity.

6.3. Foam Model Sensitivity Study

The foam model sensitivity study investigated the impact of different experimentally derived foam models on foam generation and CO₂ mobility reduction. Figure 10 shows the injection BHP for the simulation cases with three different experimentally derived foam models. See Table 4 for an overview of the foam model parameters.

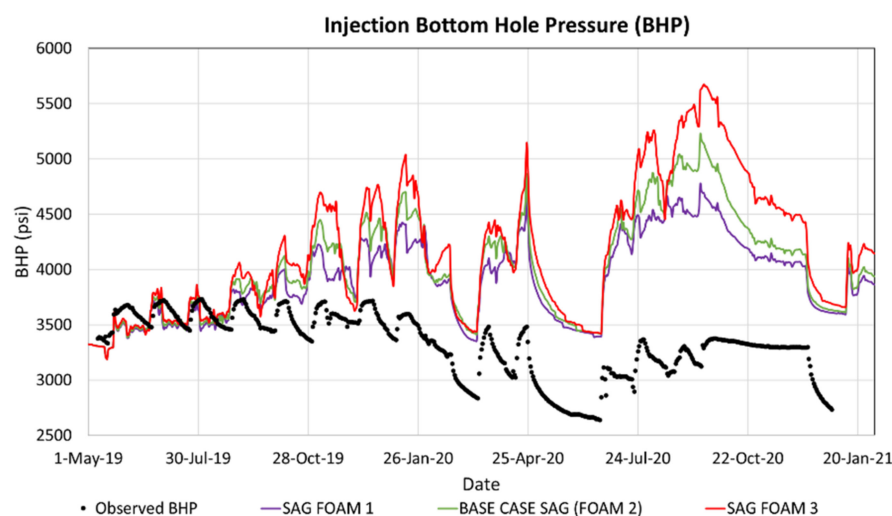


Figure 10. Injection bottom hole pressure (BHP) through time for the foam model sensitivity study. The red curve used foam model 1, the green curve is the base case SAG with foam model 2, and the purple curve used foam model 3. The observed BHP is shown as the black circles.

All three experimentally derived foam models generated foam which reduced CO₂ mobility and propagated foam into the reservoir based upon the increasing pressure build-up for each SAG cycle. Foam model 3 (Figure 10, red curve), with the highest value of *fmmob* generated the strongest foam whereas foam model 1 (Figure 10, purple curve), with the lowest *fmmob* value, generated the weakest foam relative to other cases. Thus, the most significant foam model parameter impacting injection BHP in the studied cases was *fmmob*. It was determined that the base case foam model *fmmob* parameter would be tuned to the observed BHP data to shed light on field-scale foam generation and propagation observed during the pilot. Figure 11 shows the injection BHP for the base foam model with the tuned *fmmob* value. The tuned foam model is shown at right.

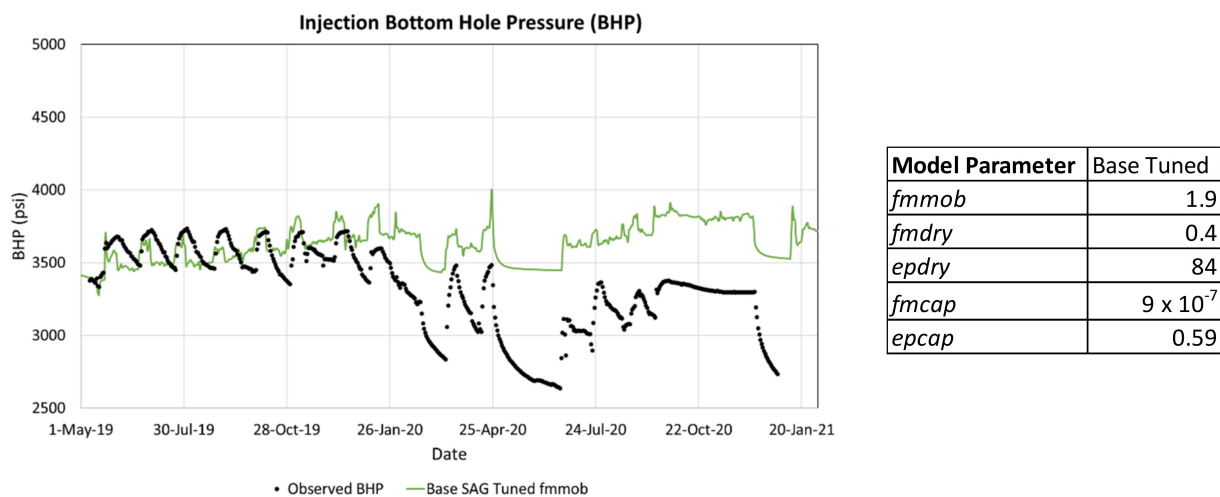


Figure 11. Injection bottom hole pressure (BHP) through time for the tuned base foam model (green curve). The observed BHP is shown as the black circles.

Reducing the *fmmob* value of the base case foam model brought the simulated BHP in closer agreement with the observed BHP response (Figure 11, black circles). Therefore, this case was used to evaluate field-scale foam propagation during the pilot. Figure 12 shows the simulated foam concentration in a 2D slice (*r-z*) of the radial model from before the pilot (Figure 12a), after the 1st SAG cycle (Figure 12b), after the 5th SAG cycle (Figure 12c), and after the 11th (final) SAG cycle (Figure 12d). Injection was from left to right in each figure. The permeability distribution is shown Figure 4b.

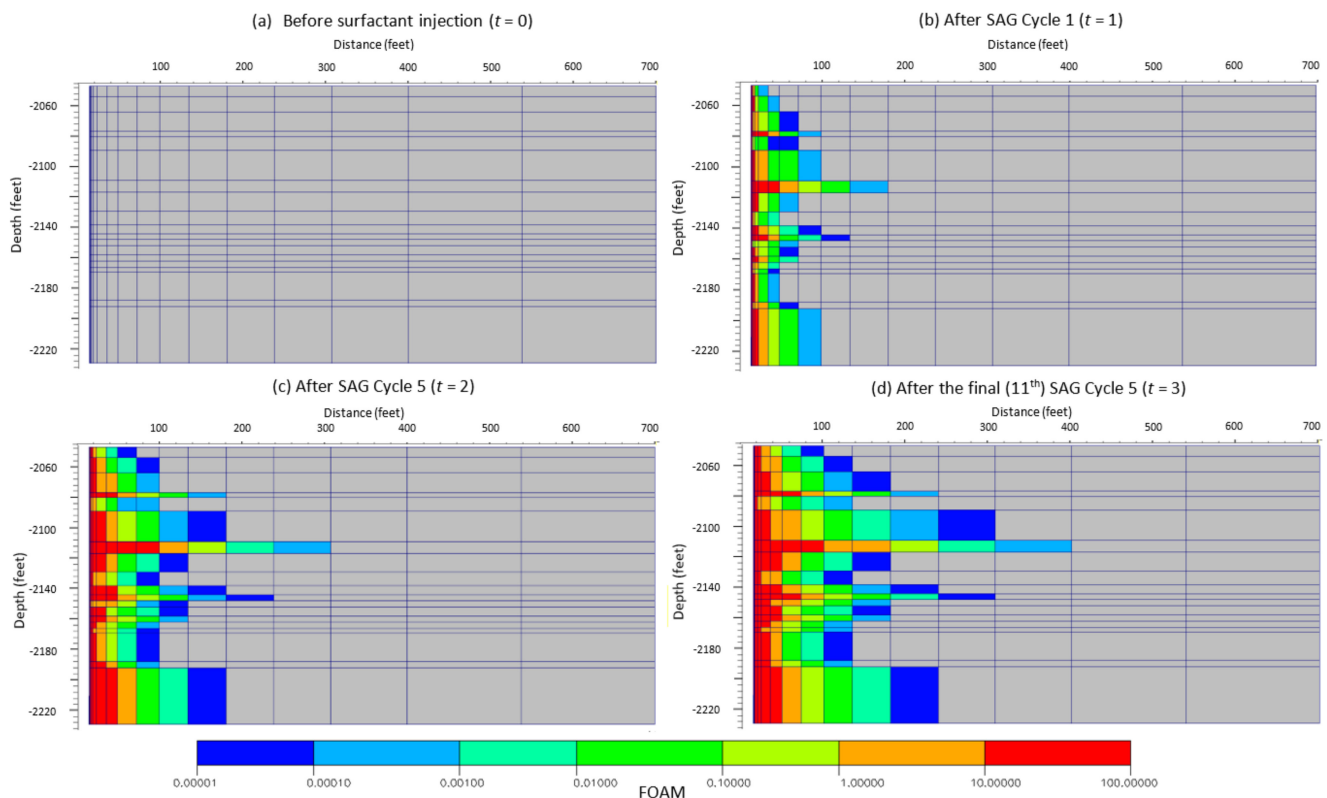


Figure 12. Foam concentration in a 2D slice (*r-z*) of the radial simulation model from (a) before surfactant injection, (b) after the 1st surfactant-alternating-gas (SAG) cycle, (c) after the 5th SAG cycle, and (d) after the 11th (final) SAG cycle. Injection was from left to right in each figure.

Figure 12b shows that foam propagated nearly 200 ft through the highest permeability layer after injection of the first SAG cycle. Foam continued to propagate as SAG injection continued, reaching a peak distance of 400 ft from the injection well (Figure 12d). Foam propagation distance was directly linked to permeability, with the highest permeability layers propagating foam the furthest. Foam more readily generates and propagates in higher permeability layers due to decreased capillary pressure.

7. Conclusions

This work presented a multiscale experimental and numerical investigation of CO₂ foam mobility control. CO₂ foam generation, strength, and propagation were evaluated at the core-scale at reservoir conditions and in a field-scale radial simulation model representing a recently completed CO₂ foam field pilot. The main objective of the experimental work was to evaluate foam generation, strength, and propagation during unsteady-state surfactant-alternating-gas (SAG) injection at reservoir conditions. The SAG injection rapidly generated foam upon the introduction of surfactant into the system. The apparent viscosity of the SAG continually increased with each subsequent SAG cycle indicating continued foam generation and propagation into the core. During a period of prolonged CO₂ injection, after SAG injection, the highest apparent viscosity value was reached before foam was destroyed in an effective drainage process, resulting in foam dry-out. Overall, the maximum apparent viscosity of the SAG was 146 cP, whereas the maximum apparent viscosity of an identical water-alternating-gas (without surfactant) injection was 2.4 cP. The laboratory methodology captured unsteady-state CO₂ foam flow and sheds light on field-scale CO₂ foam flow.

The radial reservoir simulation model investigated foam generation, strength, and propagation during a recently completed field pilot. The objective was to tune the model to match the observed bottom hole pressure (BHP) data from the foam pilot. The simulated BHP values for the base case SAG were higher than the baseline WAG, indicating that foam was generated with surfactant present. However, the base case SAG's simulated BHP values were significantly higher than the observed BHP from the pilot. This suggests that the foam generated during the pilot was not as strong as observed in laboratory studies. The foam model sensitivity study investigated the impact of different experimentally derived foam models on foam generation and strength. The most significant foam model parameter impacting injection BHP in the studied cases was the reference mobility reduction factor (*fmmob*). A reasonable match was achieved by tuning the reference mobility reduction factor. The model included a method to capture foam dry-out in the near wellbore region and indicated that foam had propagated approximately 400 ft from the injection well, more than halfway to the nearest producer, at the end of pilot injection.

Author Contributions: Conceptualization, Z.P.A.; methodology, Z.P.A., A.S. and M.K.; investigation, Z.P.A., A.S. and M.K.; writing—original draft preparation, Z.P.A.; writing—review and editing, A.S., M.K. and A.G.; supervision, Z.P.A. and A.G.; funding acquisition, Z.P.A. and A.G. All authors have read and agreed to the published version of the manuscript.

Funding: This research was funded by The Norwegian Research Council project number 249742.

Institutional Review Board Statement: Not applicable.

Acknowledgments: The authors acknowledge industry partners: Shell Global Solutions, TOTAL E&P USA, Equinor ASA and Occidental Petroleum. The authors also thank the field operator.

Conflicts of Interest: The authors declare no conflict of interest.

Nomenclature

f_g	Gas fraction or foam quality
ft	Feet
cP	Centipoise
K	Permeability
mD	Millidarcy
D	Darcy
MPa	Megapascal
Psig	Pound per square inch, gauge
rb/day	Reservoir barrels per day
ft/day	Foot per day
t	Time
S_{or}	Residual oil saturation, fraction of pore volume
f_{mmob}	Foam model, maximum gas mobility reduction factor
f_{mdry}	Foam model parameter in Fwater
f_{pdry}	Foam model parameter in Fwater
f_{msurf}	Foam model parameter in Fsurf
f_{psurf}	Foam model parameter in Fsurf
f_{mcap}	Foam model parameter in Fshear
f_{pcap}	Foam model parameter in Fshear
FM	Foam model, mobility reduction factor
k_{rg}^{nf}	Gas relative permeability with no foam

Abbreviations

CCUS	Carbon capture, utilization, and storage
CCS	Carbon capture and storage
EOR	Enhanced oil recovery
SAG	Surfactant-alternating gas
WAG	Water-alternating gas
DHPG	Down-hole pressure gauge
BHP	Bottom hole pressure
wt%	Weight percentage
IWTT	Interwell CO ₂ tracer test
HCPV	Hydrocarbon pore volume

References

- Bernard, G.G.; Holm, L.W.; Harvey, C.P. Use of Surfactant to Reduce CO₂ Mobility in Oil Displacement. *SPE J.* **1980**, *20*, 281–292. [[CrossRef](#)]
- Blaker, T.; Aarra, M.G.; Skauge, A.; Rasmussen, L.; Celius, H.K.; Martinsen, H.A.; Vassenden, F. Foam for gas mobility control in the Snorre field: The FAWAG project. *SPE Reserv. Eval. Eng.* **2002**, *5*, 317–323. [[CrossRef](#)]
- Enick, R.M.; Olsen, D.K.; Ammer, J.R.; Schuller, W. Mobility and Conformance Control for CO₂ EOR via Thickeners, Foams, and Gels—A Literature Review of 40 Years of Research and Pilot Tests; SPE-154122-MS. In Proceedings of the SPE Improved Oil Recovery Symposium, Tulsa, OK, USA, 14–18 April 2012. [[CrossRef](#)]
- Føyen, T.; Brattækås, B.; Fernø, M.A.; Barrabino, A.; Holt, T. Increased CO₂ storage capacity using CO₂-foam. *J. Greenh. Gas Control* **2020**, *96*, 103016. [[CrossRef](#)]
- Falls, A.H.; Hirasaki, G.J.; Patzek, T.W.; Gauglitz, D.A.; Miller, D.D.; Ratulowski, T. Development of a Mechanistic Foam Simulator: The Population Balance and Generation by Snap-Off. *SPE Res. Eng.* **1988**, *3*, 884–892. [[CrossRef](#)]
- Rossen, W.R. Foams in Enhanced Oil Recovery. In *Foams Theory, Measurements, and Applications*; Prud'homme, R.K., Khan, S.A., Eds.; Marcel Dekker, Inc.: New York, NY, USA, 1996; Volume 57, Chapter 11; pp. 414–464.
- Friedmann, F.; Jensen, J.A. Some Parameters Influencing Formation and Propagation of Foam in Porous Media. In Proceedings of the SPE California Regional Meeting, Oakland, CA, USA, 2–4 April 1986. [[CrossRef](#)]
- Rossen, W.R.; Gauglitz, P.A. Percolation Theory of Creation and Mobilization of Foam in Porous Media. *AIChE J.* **1990**, *36*, 1176. [[CrossRef](#)]
- Ashoori, E.; Marchesin, D.; Rossen, W.R. Roles of transient and local equilibrium foam behavior in porous media: Traveling wave. *Colloids Surf. A Physicochem. Eng. Asp.* **2011**, *377*, 228–242. [[CrossRef](#)]
- Holm, L.W.; Garrison, W.H. CO₂ Diversion with Foam in an Immiscible CO₂ Field Project. *SPE Res. Eng.* **1988**, *3*, 112–118. [[CrossRef](#)]
- Huh, D.G.; Handy, L.L. Comparison of Steady and Unsteady-State Flow of Gas and Foaming Solution in Porous Media. *SPE Res. Eng.* **1989**, *4*, 77–84. [[CrossRef](#)]

12. Castillo, R.O.S. Scale up of Surfactant Alternating Gas Foam Processes. Ph.D. Thesis, Delft University of Technology, Delft, The Netherlands, 2019. [[CrossRef](#)]
13. Ma, K.; Lopez-Salinas, J.L.; Puerto, M.C.; Miller, C.A.; Biswal, S.L.; Hirasaki, G.J. Estimation of Parameters for the Simulation of Foam Flow through Porous Media. Part 1: The Dry-Out Effect. *Energy Fuels* **2013**, *27*, 2363–2375. [[CrossRef](#)]
14. Hoefner, M.L.; Evans, E.M. CO₂ Foam: Results from Four Developmental Field Trials. *SPE Res. Eng.* **1995**, *10*, 273–281. [[CrossRef](#)]
15. Chou, S.I.; Vasicek, S.L.; Pizio, D.L. CO₂ Foam Field Trial at North Ward-Estes. In Proceedings of the SPE Annual Technical Conference and Exhibition, Washington, DC, USA, 4–7 October 1992. [[CrossRef](#)]
16. Shan, D.; Rossen, W.R. Optimal Injection Strategies for Foam IOR. *SPE J.* **2004**, *9*, 132–150. [[CrossRef](#)]
17. Leeftink, T.N.; Latooij, C.A.; Rossen, W.R. Injectivity errors in simulation of foam EOR. *J. Petrol. Sci. Eng.* **2015**, *126*, 26–34. [[CrossRef](#)]
18. Alcorn, Z.P.; Fredriksen, S.B.; Sharma, M.; Rognmo, A.U.; Føyen, T.L.; Fernø, M.A.; Graue, A. An Integrated CO₂ Foam EOR Pilot Program with Combined CCUS in an Onshore Texas Heterogeneous Carbonate Field. *SPE Resv. Eval. Eng.* **2019**, *22*, 1449–1466. [[CrossRef](#)]
19. Jian, G.; Puerto, M.C.; Wehowsky, A.; Dong, P.; Johnston, K.P.; Hirasaki, G.J. Static Adsorption of an Ethoxylated Nonionic Surfactant on Carbonate Minerals. *Langmuir* **2016**, *32*, 10244–10252. [[CrossRef](#)] [[PubMed](#)]
20. Jian, G.; Alcorn, Z.P.; Zhang, L.M.; Biswal, L.S.; Hirasaki, G.; Graue, A. Evaluation of a Nonionic Surfactant Foam for CO₂ Mobility Control in a Heterogeneous Carbonate Reservoir. *SPE J.* **2020**, *25*, 3481–3493. [[CrossRef](#)]
21. Alcorn, Z.P.; Sharma, M.; Fredriksen, S.B.; Rognmo, A.U.; Fernø, M.A.; Graue, A. CO₂ Foam Field Pilot Test for EOR and CO₂ Storage in a Heterogeneous Carbonate Reservoir: Operational Design, Data Collection and Pilot Monitoring Program. In Proceedings of the 80th EAGE Annual Conference and Exhibition, Copenhagen, Denmark, 11–14 June 2018. [[CrossRef](#)]
22. Alcorn, Z.P.; Karakas, M.; Graue, A. CO₂ Foam Pilot in a Heterogeneous Carbonate Reservoir: Analysis and Results. In Proceedings of the SPE Improved Oil Recovery Conference, Virtual, 25–28 April 2022. [[CrossRef](#)]
23. Al-Menhali, A.; Krevor, S. The Impact of Crude Oil Induced Wettability Alteration on Remaining Saturations of CO₂ in Carbonate Reservoirs: A Core Flood Method. In Proceedings of the 2016 SPE Europec featured at 78th EAGE Conference and Exhibition, Vienna, Austria, 30 May–2 June 2016.
24. Jones, S.A.; Laskaris, G.; Vincent-Bonnieu, G.; Farajzadeh, R.; Rossen, W.R. Surfactant Effect on Foam: From Core Flood Experiments to Implicit-Texture Foam-Model Parameters. In Proceedings of the SPE Improved Oil Recovery Conference, Tulsa, OK, USA, 11–13 April 2016.
25. Karakas, M.; Alcorn, Z.P.; Graue, A. Pressure Measurements for Monitoring CO₂ Foam Pilots. *Energies* **2022**, *15*, 3035. [[CrossRef](#)]
26. Sharma, M.; Alcorn, Z.; Fredriksen, S.; Fernø, M.; Graue, A. Numerical Modeling Study for Designing CO₂-foam Field Pilot. In Proceedings of the IOR 2017—19th European Symposium on Improved Oil Recovery, Stavanger, Norway, 24 April 2017.
27. Cheng, L.; Reme, A.; Shan, D.; Coombe, D.; Rossen, W. Simulating Foam Processes at High and Low Foam Qualities. In Proceedings of the SPE/DOE Improved Oil Recovery Symposium, Tulsa, OK, USA, 3 April 2000.
28. Farajzadeh, R.; Andrianov, A.; Krastev, R.; Hirasaki, G.; Rossen, W. Foam–oil interaction in porous media: Implications for foam assisted enhanced oil recovery. *Adv. Colloid Interface Sci.* **2012**, *183–184*, 1–13. [[CrossRef](#)] [[PubMed](#)]
29. Sharma, M.; Alcorn, Z.P.; Fredriksen, S.B.; Fernø, M.A.; Skjæveland, S.; Graue, A. Model Calibration for Forecasting CO₂-Foam EOR Field Pilot Performance in a Carbonate Reservoir. *Pet. Geosci.* **2020**, *26*, 141–149. [[CrossRef](#)]
30. Rognmo, A.U.; Fredriksen, S.B.; Alcorn, Z.P.; Sharma, M.; Føyen, T.; Eide, G.A.; Fernø, M. Pore-to-Core EOR Upscaling for CO₂ Foam for CCUS. *SPE J.* **2019**, *24*, 2793–2803. [[CrossRef](#)]
31. Lake, L.W. *Enhanced Oil Recovery*; Society of Petroleum Engineers: Richardson, TX, USA, 2010.
32. Chou, S.I. Conditions for Generating Foam in Porous Media. In Proceedings of the SPE Annual Technical Conference and Exhibition, Dallas, TX, USA, 6–9 October 1991.
33. Ransohoff, T.C.; Radke, C.J. Mechanisms of Foam Generation in Glass-Bead Packs. *SPE Res. Eng.* **1988**, *3*, 573–585. [[CrossRef](#)]
34. Patzek, T.W. Field Applications of Steam Foam for Mobility Improvement and Profile Control. *SPE Res. Eng.* **1996**, *11*, 79–86. [[CrossRef](#)]